Anodic Decomposition of Trimethylboroxine as Additive for High Voltage Li-Ion Batteries

A. Freiberg,[a] M. Metzger,[a,*] D. Haering,[a] S. Bretzke,[b] S. Puravankara,[b] T. Nilges,[b] C. Stinner,[c] C. Marino,[a,,z] and H. A. Gasteiger[a,***]**

[a]*Chair of Technical Electrochemistry, Chemistry Department, Technische Universität München, 85748 Garching, Germany*
[b]*Synthesis and Characterization of Innovative Materials, Chemistry Department, Technische Universität München, 85748 Garching, Germany*
[c]*BMW AG, 80788 München, Germany*

Trimethylboroxine (TMB) is used as an additive in the electrolyte for improving the performance of $LiCoPO_4$ (LCP) in Li-ion batteries. In this work, the role and behavior of TMB are investigated by cyclic voltammetry (CV), impedance spectroscopy (EIS) and on line electrochemical mass spectroscopy (OEMS). It was found that TMB oxidizes from 4.6 V and a low amount in the electrolyte is necessary to obtain good performance. On one hand, its oxidation produces boron trifluoride (BF_3), phosphorylfluoride (POF_3) and carbanion (CH_3^-) linked to a huge increase in impedance. Based on these results, a complete oxidation mechanism is proposed. The catalytic effect of the TMB decomposition products on carbonate polymerization could enhance the performance of LCP. On the other hand, an unexplained water and/or HF release was detected. Further experiments need to be done.
© The Author(s) 2014. Published by ECS. This is an open access article distributed under the terms of the Creative Commons Attribution 4.0 License (CC BY, http://creativecommons.org/licenses/by/4.0/), which permits unrestricted reuse of the work in any medium, provided the original work is properly cited. [DOI: 10.1149/2.0011501jes] All rights reserved.

Manuscript submitted August 6, 2014; revised manuscript received October 3, 2014. Published October 30, 2014. This was Paper 295 presented at the Orlando, Florida, Meeting of the Society, May 11–15, 2014.

Rechargeable lithium batteries were first developed with lithium metal as a negative electrode (anode) and several positive electrode (cathode) materials like Li/MnO_2[1] or $Li/LiTiS_2$.[2] Due to safety issues related to dendrite formation with lithium metal anode, the first Li-ion batteries were commercialized by Sony in 1991 using graphite anodes.[3] Later on, layered-oxide based cathode materials like $LiCoO_2$ were developed, which have specific capacities and specific energies of ≈170 mAh/g_{LiCoO2} and ≈600 mWh/g_{LiCoO2}, respectively. In order to improve battery safety, cost and energy density, recent research has focused on new electrode materials. On the cathode side, numerous spinel structure materials were tested and showed good electrochemical performance.[4] In 1997, phospho-olivine cathode materials of the general formula $LiMPO_4$ (M = 3d-transition metal) emerged with the discovery of $LiFePO_4$ (LFP) by Goodenough's group,[5] which generally have more safety characteristics due to the strong P-O bond preventing O_2 release at high potential/temperature (problematic with layered oxides). So far, more than 1200 patents have been filed for phospho-olivines.[6] LFP has a theoretical specific capacity of 171 mAh/g_{LFP} and the oxidation from Fe^{II} to Fe^{III} takes place at 3.45 V, resulting in a specific energy of ≈590 mWh/g_{LFP}. While offering improved safety, its specific energy is very similar to $LiCoO_2$, so that with respect to energy density, LFP offers no improvement over $LiCoO_2$.

One approach toward improved energy density required for electric vehicle applications would be the use of $LiCoPO_4$ (LCP) cathode material, which promises a theoretical specific energy of ≈800 mWh/g_{LCP} based on a charge/discharge voltage of ≈4.85 V vs. Li/Li^+ and a theoretical specific capacity of 167 mAh/g_{LCP}.[7,8] However, the reported electrochemical performance of LCP, synthesized by many different routes, does not reach the theoretical specific capacity, shows low coulombic efficiency, and exhibits poor cycling stability. For example, Ni et al.[9] synthetized carbon-coated LCP material by a sol gel route which gave a specific capacity of 131 mAh/g_{LCP} at 0.1 C in the 1st cycle and lost 25% of its initial capacity after only 40 cycles. Slightly higher initial discharge capacities of 145 mAh/g_{LCP} at 0.1 C in the 1st cycle were obtained for an LCP-carbon composite synthesized by a solid state route, but similar capacity fading was observed.[10] The addition of a constant-voltage (CV) step at the end of charge was shown to improve the charge/discharge cycling performances,[11] but capacity fading was also very fast (20% of capacity loss after only 10 cycles). Kang et al.[12] demonstrated that cobalt can migrate into the lithium sites during the first delithiation of LCP, thereby blocking lithium ion diffusion, which in turn was suggested to cause the observed capacity fading; iron doping was claimed to suppress cobalt migration and to improve cycle-stability. On the other hand, Markevic et al.[13] proposed that capacity fading might largely be related to the reaction of fluoride ions (present in electrolytes with $LiPF_6$ salt) with LCP through a nucleophilic attack of F^- on the P atoms of delithiated (charged) LCP, owing to the instability of the high-spin Co^{3+} in $CoPO_4$. This hypothesis was substantiated by the reduced capacity fading when using a quartz separator compared to a polyethylene separator, assuming that quartz would serve as a fluoride ion scavenger.[14] The use of different additives in the electrolyte should prevent the electrode material from electrolyte corrosion and limit the capacity decrease. Recently, the same group[15] reported improved performance by using a conventional $LiPF_6$ based electrolyte with trimethylboroxine (TMB) additive and fluoroethylene carbonate (FEC) as co-solvent: a capacity of 100 mAh/g_{LCP} was maintained after 100 cycles at a rate of 0.2 C. Based on XPS studies, they concluded that FEC creates a better SEI layer on the cathode, but the mechanism leading to the reduced capacity fading by the addition of TMB could not be fully resolved.

To gain more insight into the positive effect of TMB on the capacity fading of LCP, the present work examines the anodic decomposition pathways of TMB using cyclic voltammetry (CV), electrochemical impedance spectroscopy (EIS), and on-line electrochemical mass spectrometry (OEMS).[16] We will show that small amounts of TMB substantially improve the cycle life of LCP, while larger amounts lead to a very large increase of the high-to-medium frequency resistance of LCP, resulting in accelerated capacity fading. The essentially complete anodic decomposition of TMB at the charge/discharge potential of LCP proceeds through the formation of BF_3 and POF_3. The subsequent reaction of BF_3 and other TMB decomposition fragments (CH_3^- carbanions) leads to the degradation of alkyl carbonates, which we believe causes the substantial increase of the high-to-medium frequency resistance of LCP via the formation of a passivating surface film when large amounts of TMB additive are used.

Experimental

LCP synthesis and characterization.— $LiCoPO_4$ was synthesized using a conventional solid state route according to Jang et al.[17]

*Electrochemical Society Student Member.
**Electrochemical Society Active Member.
***Electrochemical Society Fellow.
zE-mail: Cyril.marino@tum.de

Stoichiometric amounts of $LiOH \cdot H_2O$ (crystals, 99%, Fluka), $NH_4H_2PO_4$ (crystals, 99,995%, Puratonic) and Co_3O_4 (powder, 99%, Alfa Aesear) were used. To remove the crystal water, the educts were initially homogenized in a mortar and precalcined at 673 K for 12 h. Subsequently, the educts were homogenized at 400 rpm in a planetary ball mill and then calcined at 1073 K under argon for 10 h in order to obtain pure single phase $LiCoPO_4$. After the synthesis, a particle size reduction step was conducted, consisting of ball milling (Fritsch Pulverisette 7) in a 45 mL ZrO_2 jar with ZrO_2 balls (1 mm diameter) at 1100 rpm for 1.5 h, followed by annealing at 873 K for 1h under argon.

The powder diffraction data of the samples were collected with a STOE StadiP powder diffractometer with a Mo-K_α X-ray source (Ge(111) monochromator, $\lambda = 0.7093$ Å) and a Dectris Mythen 1 K detector. The measurements were done at 298 K in a 2θ range of 5° to 60° (step of 0.015° 2θ, 25 s/step, 3 ranges). The Rietveld refinement of the data was done with the software Jana2006.[18]

The specific surface area was measured by N_2-adsorption BET (Quantachrome Autosorb iQ) after outgassing of the sample at 150°C for 16 h.

Electrode preparation.— For electrode preparation, the synthesized LCP was mixed with Super-C65 (TIMCAL) and PVdF (Kynar HSV 900, ARCHEMA) at a weight ratio of 80:10:10 (LCP:SuperC:PVdF). Upon addition of NMP (Sigma Aldrich), an ink was prepared by ball milling (Fritsch Pulverisette 7) in a 20 mL ZrO_2 jar with ZrO_2 balls (10 mm diameter) at 180 rpm for 1 h and then coated onto aluminum foil (18 μm, MTI corporation) using a gap-bar coater (RK Print). After drying at room temperature, electrodes with 10 mm diameter were punched, pressed under vacuum at 380 MPa (KBr-press, PerkinElmer), and dried at 120°C under vacuum in a Glass Oven (Büchi drying Oven 585). The LCP loading of all the electrodes prepared for this study was within the range of 4.10 ± 0.3 mg_{LCP}/cm^2 (the exact weight for each electrode was determined to ± 0.05 mg/cm^2). Carbon electrodes coated onto aluminum foil and consisting of 50%$_{wt}$ Super-C65 (TIMCAL) and 50%$_{wt}$ PVdF were also prepared by the same process, but without subsequent compression of the electrodes. For OEMS experiments, carbon electrodes at a loading of ≈0.6 mg/cm^2 were prepared by spreading similar inks (50%$_{wt}$ Super-C65 and 50%$_{wt}$ PVdF) onto aluminum foam disks with 15 mm diameter (600 μm thickness, 6–8% density; Duocel).

Electrolyte and battery test cell assembly.— Electrolytes used for this study were 1 M $LiPF_6$ in EC:DMC (1:1 wt:wt) (LP30, Merck); either without additive or with the addition of 0.2%$_{wt}$, 0.5%$_{wt}$, 1 %$_{wt}$, and 3%$_{wt}$ of TMB (99%, Aldrich). The water content of each electrolyte determined by Karl-Fischer titration was below 10 ppm.

For charge/discharge cycle-life investigations, two-electrode Swagelok T-cells were assembled in a argon filled glove-box (water and oxygen below 0.1 ppm) using two glass fiber separators (250 μm, VWR) and 80 μl of electrolyte. We note that glass fiber separator is easily wetted by LP30 electrolyte and could act as –F scavenger.[14] A 450 μm thick lithium foil (Rockwood Lithium) with a diameter of 11 mm was used as counter electrode. Tests were conducted with a battery cycler (Maccor, Series 4000) using the following procedure: 12 h rest at open circuit voltage (OCV), then two formation cycles at a constant current rate of C/15, followed by cycling at C/2 between 3.5 and 5.2 V without any constant-voltage step.

EIS and CV experiments were carried out with three-electrode Swagelok T-cells with lithium foil counter and reference electrodes and with three glass fiber separators wetted with 120 μl of electrolyte. EIS measurements were employed to study the high-to-medium frequency resistance of LCP electrodes (working electrode), following a test procedure similar to the one used for the above described charge/discharge cycling experiments: 12 h of OCV, then two formation cycles at C/15, followed by 20 cycles at C/2; impedance spectra between 0.1 Hz and 500 kHz (10 mV voltage perturbation) were obtained after every charge and discharge at potentials of 5.2 and 3.5 V, respectively (after a brief constant-voltage hold at the cut-off voltages prior to recording the impedance spectra). Carbon working electrodes were used to study electrolyte decomposition (with and without TMB additive) by CV, recording three cycles between OCV and 5.5 V at 0.02 mV/s. All EIS and CV measurements were conducted with a VMP 3 potentiostat (Biologic).

OEMS experiment.— For in-situ gas analysis by on-line electrochemical mass spectrometry (OEMS), the battery test cells were assembled in a special cell hardware, described recently.[16] It consists of a 316Ti stainless steel anode current collector and a stainless steel mesh (316 SS) cathode current collector (0.22 mm diameter wire, 1.0 mm openings; Spörl KG), which is contacted and compressed by a compression spring (316 SS; Lee Springs). The above described carbon/aluminum-foam served as working electrode and was contacted by the stainless steel mesh; a 17 mm diameter lithium foil (Rockwood Lithium, 450 μm) was placed onto the stainless steel anode current collector. Between the electrodes, two 28 mm diameter glass fiber separators (250 μm, VWR) were placed and 320 μl of electrolyte were added. After assembly and sealing in the glove-box, the cell was placed into a climate chamber held at 25°C (KB 20, Binder). A crimped capillary leak (Vacuum Technology Inc.) connects the OEMS cell to the mass spectrometer system (Pfeiffer Vacuum QMA 410), permitting a constant flow of ≈1 μl/min from the cell head space (9.5 ml) to the cross-beam ionization source of the mass spectrometer. The OEMS system is equipped with a secondary electron multiplier (SEM), allowing the detection of masses between 1 and 128 amu. To avoid signal fluctuations due to minor pressure/temperature changes, all mass signal currents, I_Z, were normalized to the mass current of the ^{36}Ar isotope, I_{36}. A linear potential scan from OCV to 5.3 V at 0.2 mV/s (Gamry Series G300 potentiostat) was used to study the decomposition of electrolyte with and without TMB additive via OEMS.

Results

Physical-chemical characterization of LCP.— The X-ray diffraction pattern and the SEM picture of the synthetized LCP after the particle size reduction step and the final annealing at 600°C are shown in Figure 1. Homogeneous spherical LCP particles of 50-60 nm are observed by SEM, which is in good agreement with the measured BET value of 24 m^2/g (spherical approximation: $d_{average} = 6/(24\ m^2/g \times 3.6 \cdot 10^6\ g/m^3) = 65$ nm). The XRD pattern of the synthetized compound reveals sharp Bragg peaks, indicative of a highly crystalline sample, which could all be indexed to an olivine-type $LiCoPO_4$ cell (space group *Pnma* – ICSD-99862). The refined lattice parameters of the unit cell (a = 10.1844[5] Å, b = 5.9138[3] Å, c = 4.6936[2] Å, corresponding to a cell volume of 282.7[3] $Å^3$) are in good agreement with the literature.[17–19] No side phases were detected by XRD.

Anodic stability via cyclic voltammetry experiments.— CV experiments were carried out on carbon electrodes in order to study the anodic stability of the electrolyte containing 0.2% and 1% TMB. The standard electrolyte (LP30) without TMB was used as a reference. The results of the first positive-going (anodic) scan at 0.02 mV/s are shown in Figure 2a. While no significant anodic currents are observed until ≈4.7 V without TMB additive, substantial oxidation currents initiate at ≈4.6 V in the electrolyte containing 1% TMB, increasing to ≈80 μA (≈100 $\mu A/cm^2$) at the positive potential limit of 5.3 V. Lower anodic currents and an analogous current vs. potential behavior are observed for the electrolyte with 0.2% TMB, also showing a potential peak at ≈4.9 V followed by an exponential current increase at the positive voltage limit. While part of the oxidation current will be due to the corrosion of the aluminum current collector,[20] the substantial increase of the oxidation currents at any given potential with TMB concentration suggests that a large fraction of the observed anodic currents are due to the oxidative decomposition of TMB. This will be demonstrated by OEMS data later on.

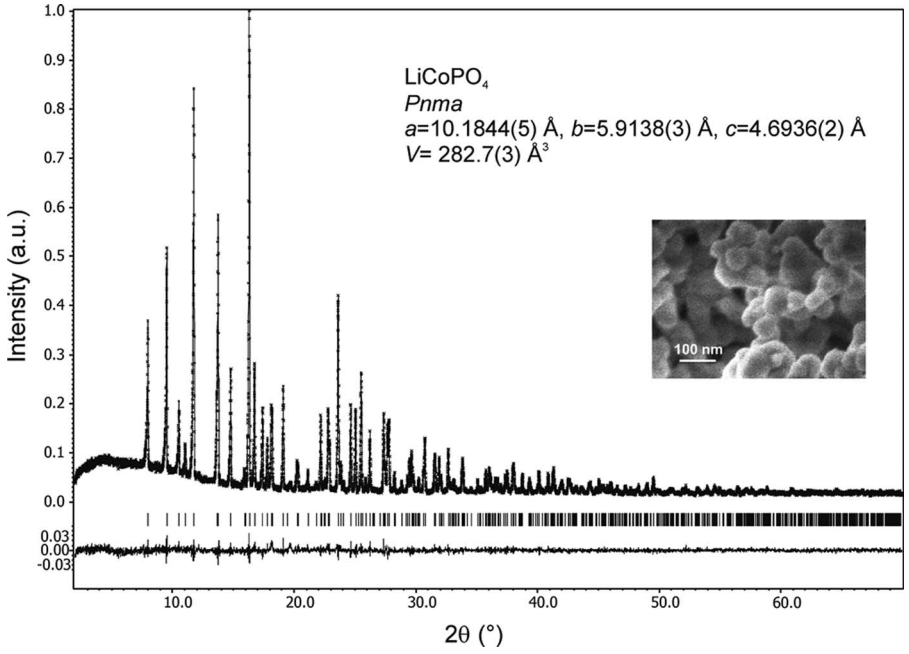

Figure 1. X-ray diffraction pattern and SEM picture of synthesized $LiCoPO_4$ powder after the particle-size reduction step.

Figure 2b compares the 3rd voltammetric cycle in the electrolytes used in the previous CV experiment. While the current decreases only very little from the 1st to the 3rd cycle in TMB-free electrolyte, the oxidation currents decrease substantially by a factor of two in the electrolyte with 0.2% TMB and 1% TMB. This suggests that TMB can be oxidatively decomposed either completely within the examined potential range or partially due to the formation of a passivating layer.

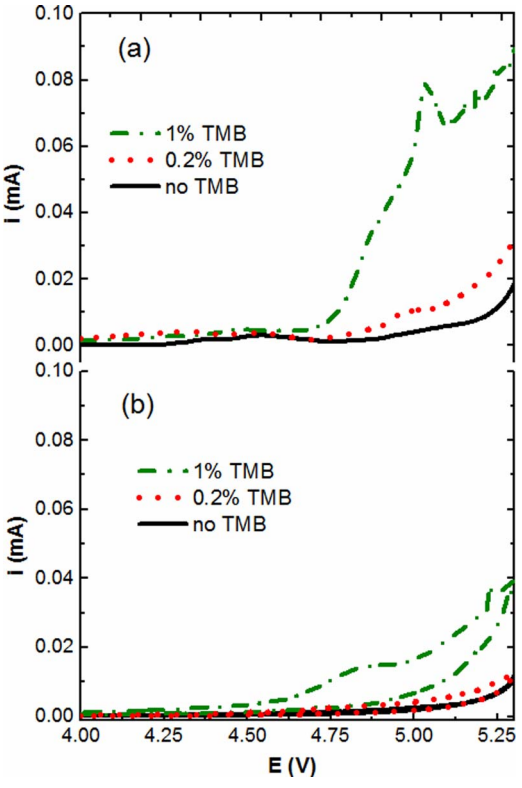

Figure 2. Cyclic voltammograms of carbon electrodes in electrolyte (1 M $LiPF_6$ in EC:DMC (1/1 w/w)) containing different amounts of TMB: a) 1st positive-going scan; b) 3rd positive and negative-going scans. CVs were conducted at 0.02 mV/s at room temperature.

We note that the current values in TMB-free electrolyte and in the electrolyte with 0.2% TMB are similar in the 3rd cycle. Interestingly, the electrolyte with 1% TMB does not reach the current corresponding to the electrolyte without additive. Probably, a high amount of TMB leads to a higher degradation or a lower efficiency in the building of the passivating layer. Next experiments should help to understand this observation.

Galvanostatic charge/discharge cycling with and without TMB.— To determine the effect of TMB on the capacity fading of LCP, we chose a galvanostatic cycling procedure between 3.5 and 5.2 V with two initial formation cycles at low rate of C/15, followed by fast cycling at C/2 ($\equiv$0.34 $\pm$ 0.03 mA/cm^2). At C/2 rate cycling following the two slow formation cycles, the contribution from TMB oxidation to the charge/discharge capacities should be negligible based on the CV data in Figure 2b. The evolution of the discharge capacity versus cycle number for LCP electrodes in electrolyte containing different concentrations of TMB is depicted in Figure 3, illustrating

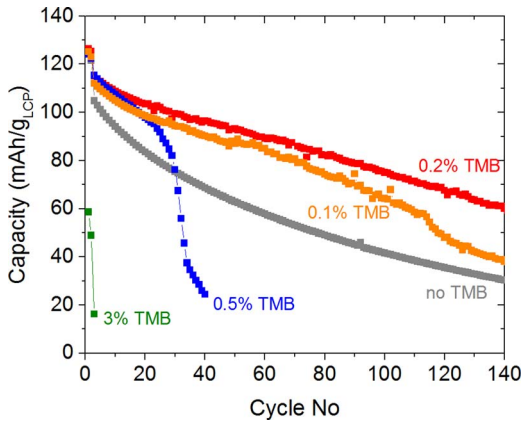

Figure 3. Specific discharge capacity (in mAh/g_{LCP}) vs. cycle number of LCP electrodes in electrolyte (1 M $LiPF_6$ in EC:DMC (1/1 g/g)) containing different amounts of TMB indicated in the figure. The first two galvanostatic cycles (formation) were conducted at C/15 rate, followed by galvanostatic cycles at C/2 rate; the lower and upper cut-off voltages were 3.5 and 5.2 V, respectively.

Table I. i) Number of cycles with specific discharge capacities of ≥100 mAh/g_{LCP} for 1 M $LiPF_6$ in EC:DMC (1/1 g/g)) electrolyte with different amounts of TMB additive. Galvanostatic cycles between 3.5 and 5.2 V at C/2 rate after two initial formation cycles at C/15 rate. The discharge capacities in the first cycle for all electrolytes are 125 ± 2 mAh/g_{LCP}; ii) Irreversible capacity loss at the 1st cycle in electrolyte with different amounts of TMB additive.

$\%_{wt}$ TMB in LP30	0	0.1	0.2	0.5	3
i) number of cycles with ≥100 mAh/g_{LCP}	6	18	30	10	0
ii) Irreversible capacity loss 1st cycle (mAh/g_{LCP})	57	94	94	92	1095

the strong effect of TMB additive on capacity fading. At the first cycle, a capacity of 125 ± 2 mAh/g_{LCP} is obtained in all the electrolytes except those containing 3% TMB, which only yields ≈60 mAh/g_{LCP}. Once the current is increased after the two formation cycles, higher capacity fading is noticed for the TMB-free electrolyte compared to electrolytes containing between 0.1% and 0.5% TMB. The lowest capacity fading is observed for the electrolyte containing 0.2% TMB. Table I summarizes the number of cycles for which ≥100 mAh/g_{LCP} can be maintained throughout this cycling procedure, with a maximum of 30 cycles (2 at C/15 followed by 28 at C/2) for the electrolyte with 0.2% TMB and substantially lower cycle numbers for higher or lower TMB concentrations. This may be compared with the galvanostatic charge/discharge cycling at C/5 for LCP conducted by Sharabi et al.,[15] where in the same standard electrolyte without additive or co-solvent the specific capacity drops below 100 mAh/g_{LCP} in the first cycle. Using FEC co-solvent (i.e., 1 M $LiPF_6$ in FEC:DMC (1:4 wt:wt)), 100 mAh/g_{LCP} can only be maintained over 4 cycles, while 100 cycles at ≥100 mAh/g_{LCP} can be obtained when 0.5% TMB are added to the FEC:DMC electrolyte (this may be compared to the 30 cycles we obtain with 0.2% TMB, see Table I). Unfortunately, addition of FEC as co-solvent to our electrolyte with 0.2% TMB did not improve the number of cycles at ≥100 mAh/g_{LCP}.

At first glance, it is surprising that Sharabi et al.[15] obtain the lowest capacity fading with 0.5% TMB in their LCP half-cell measurements (using a lithium metal counter electrode as in our study) and that they suggest 0.5–1% TMB to the optimum concentration range, while we observe very high capacity fading with 0.5% TMB (see Figure 3). This, however, can be easily explained when considering the volume of electrolyte per milligram of active material, which is 25 ± 2 $\mu L_{electrolyte}/mg_{LCP}$ in our experiments instead of 5 $\mu L_{electrolyte}/mg_{LCP}$ in the work by Sharabi et al. in conjunction with the assumption that the critical variable is not the additive concentration in the electrolyte, but the additive/active-material mass ratio. The latter is identical for the optimum 0.1–0.2% TMB concentration in our case and the optimum TMB concentration of 0.5–1% reported by Sharabi et al., namely 0.03–0.06 mg_{TMB}/mg_{LCP}. (using a density for the reference electrolyte of 1.3 g/cm^3). In general, these calculations point out that the optimization of the additive concentration in the electrolyte has to take into account the additive/active-material mass ratio in the assembled cell, and thus depends on the ratio of electrolyte volume to active-material mass, which is vastly different for small-scale test cells (5–25 $\mu l_{electrolyte}/mg_{active\text{-}material}$, see above) vs. commercial cells (0.3–0.5 $\mu l_{electrolyte}/mg_{active\text{-}materials}$). Therefore, optimum additive concentrations determined from small-scale test cell evaluations would likely have to be increased by at least an order of magnitude for use in commercial cells.

Additionnaly, Table I exposes the irreversible capacity loss (ICL) for the 1st cycle in electrolyte containing different concentrations of TMB. The ICL at the 1st cycle are increasing with the TMB content. However, in electrolyte with 0.1–0.5% TMB, the ICL are similar, as well as the discharge capacities for 15 cycles. Those high values are consistent with the oxidation on charge of the TMB additive. According to CV results, a low amount of TMB (0.2% for example) leads to a higher current only in the first cycle (see Figure 2) whereas similar values are observed for the 3rd cycle. A passivation layer is probably formed during the first cycle and could be a reason of the stable ICL for the electrolyte containing 0.1–0.5% TMB. Those amounts of TMB appear to be an optimum to allow a good passivation. For higher amount of TMB, an additional mechanism is probably taking place.

LCP impedance vs. cycle number.— The following impedance analysis is aimed to gain further insights into the observed strong capacity fading at high TMB additive concentrations. The Nyquist plots of the LCP impedance (Z_{LCP}, i.e., recorded vs. the lithium metal reference electrode) at the end of discharge after the 1st cycle at C/2 rate for different electrolytes are shown in Figure 4a. The LCP impedances in the electrolyte containing no additive and 0.2% TMB are quite similar, and the frequencies at the maximum of the semi-circle are also quite similar (3–7 kHz). On the other hand, the LCP impedance in the electrolyte containing 0.5% TMB reveals a ≈10-fold larger medium-frequency resistance (see inset of Figure 4a) and a ≈10-fold lower frequency maximum of the semi-circle (0.4 kHz). Both, the larger medium-frequency resistance and the lower frequency at the maximum of the semi-circle (note: $\omega_{max} \propto 1/(R \cdot C)$) indicate an overall vastly increased charge-transfer and/or interface resistance of LCP in electrolyte with 0.5% TMB compared to 0% or 0.2% TMB.

After 20 cycles (Figure 4b), a huge increase of the LCP impedance is noted for the electrolyte containing 0.5% TMB, with a

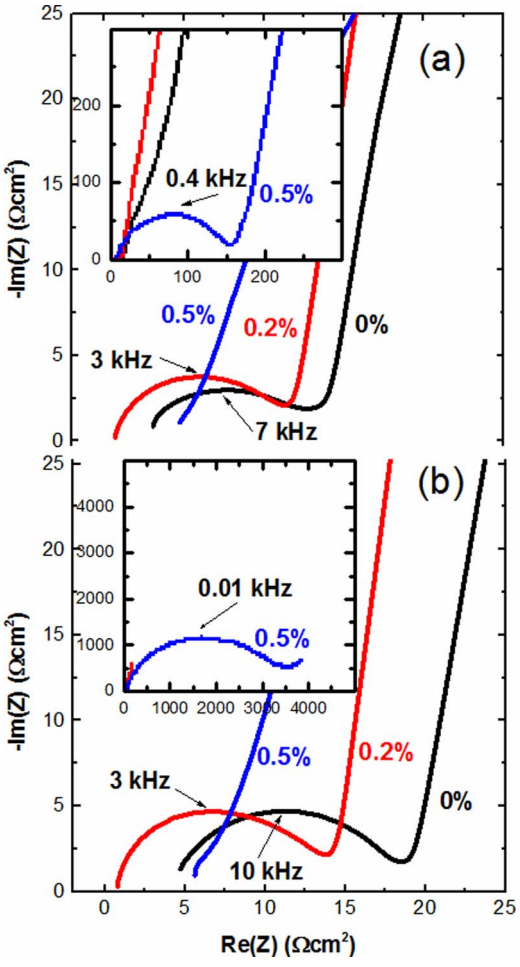

Figure 4. Nyquist plot of the LCP electrode impedance, Z_{LCP}, recorded vs. a lithium metal reference electrode in electrolyte (1 M $LiPF_6$ in EC:DMC (1/1 g/g)) with different amounts of TMB at: a) end of 1st discharge at C/2; b) end of 20th discharge at C/2. The same data are shown in the insets with different x- and y-axis scales to be able to depict the data for 0.5% TMB.

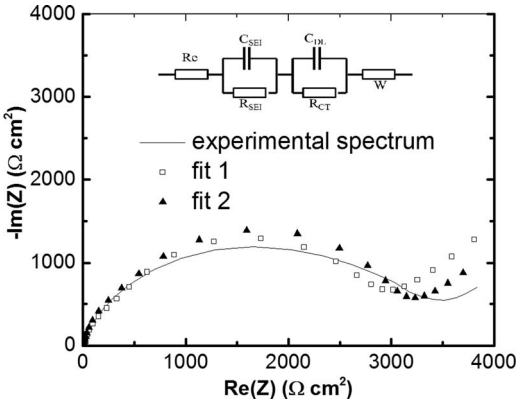

Figure 5. Fits of Nyquist plot recored at the end of 20th discharge in the electrolyte containing 0.5% TMB. Fit 1 and fit 2 refer to model fits using different initial estimates of R_{SEI} and R_{CT}. The inset depicts the equivalent circuit model proposed for the LCP interface, viz., one R/C circuit for an interfacial film represented by R_{SEI} and C_{SEI} and one R/C circuit for the charge transfer represented by R_{CT} and C_{DL}, followed by a Warburg resistance element, W, and the electrolyte resistance, R_e.

≈200-fold larger medium-frequency resistance (≈3 kΩ · cm^2) compared to the values obtained for electrolytes with 0% and 0.2% TMB (≈15 Ω · cm^2). Quite clearly, the impedance data suggest a continuous growth of a highly resistive interface layer on the LCP electrode in the presence of large amounts of TMB. This is consistent with the excessive capacity fading observed with 0.5% and 3% TMB in Figure 3.

Further analysis of the EIS spectra were done following a circuit proposed by Rajalakshmi et al.[21] for LCP electrodes (see inset of Figure 5). In this model, R_e represents the resistance of the liquid electrolyte. For the passivation layer, C_{SEI} and R_{SEI} are the capacitance and the resistance of the SEI layer on the LCP respectively. To model the electrode/electrolyte charge transfer, C_{DL} corresponds to the double layer capacitance and R_{CT} is the charge transfer resistance. Finally, W represents the Warburg impedance, representing the diffusion of charge carriers in the electrode. The fitted values for the 3 resistances after the 1st and the 20th discharge at C/2 rate are given in Table II, whereby two fits with different initial parameter estimates were used (fit 1 and fit 2). Quite clearly, the values for R_{SEI} and R_{CT} are not unique, i.e., they depend on the initial parameter estimates, which means that experimentally it is not possible to distinguish between these two values, but that its sum (($R_{SEI} + R_{CT}$), see Table II) is a more meaningful value indicating the overall impedance to charge transfer at the LCP electrode. The latter is rather small for electrolytes without TMB and with 0.2% TMB. In the case of 0.5% TMB, ($R_{SEI} + R_{CT}$) is already 10-fold larger after the 1st cycle, increasing by another factor of 10 by the end of the 20th cycle. In summary, the fitted impedance data confirm that the addition of a high amount of TMB causes a tremendous increase in the overall medium-frequency resistance ($R_{SEI} + R_{CT}$), most likely due to the formation of a thick interfacial layer. On the other hand, the electrolyte containing 0.2% TMB shows a medium-frequency resistance comparable to that of TMB-free electrolyte. This remarkable result will be discussed later.

Products derived from anodic TMB decomposition on carbon electrode.— In the following, we will examine the gas evolution products via OEMS during the anodic oxidation of 1 M $LiPF_6$ in EC:DMC without TMB and with 0.5% TMB additive using a carbon working electrode in a linear voltammetric scan experiment (0.2 mV/s) from OCV to 5.3 V. The linear sweep voltammetry (LSV) curves (Figure 6a) are very similar to what was shown in Figure 2a, displaying very large oxidation currents in the presence of TMB additive, with a potential peak near 4.9 V. The mass spectrometer currents at various m/z-values normalized by the mass spectrometer current of the ^{36}Ar isotope, I_Z/I_{36}, are shown in Figures 6b–6e. The relevant mass signals 85,44,15,19,69,31,16 arising from the anodic decomposition of the electrolyte without additive are shown in Figure 6b. Most of the mass signals start to evolve at ≈4.5 V, concomitant with the onset of the anodic current in the LSV curve (Figure 6a). Novák and coworkers[22,23] showed CO_2 (mass 44) evolution coming from electrolyte oxidation and proposed a mechanism of the oxidation of DMC which leads to CO_2 evolution. The other signals are probably related to either mass fragments of anodic oxidation products from the carbonates or from decomposition products of the $LiPF_6$ salt[24,25] (see also below discussion). However, it can be noted that the I_z/I_{36} signals for all masses are very low (below 0.15).

An order of magnitude larger mass signals are obtained with 0.5% TMB additive, and are shown in Figures 6c–6e (please note the 10-fold larger I_Z/I_{36} scale compared to Figure 6b) in order to explain the decomposition mechanism of TMB (scheme 1(a)–1(e)). The strongest signal is mass 49, which initiates at ≈4.8 V (Figure 6c) and is attributed to BF_3 release, confirmed by the concomitant appearance of mass 48, which is the expected mass-spectrometric fragment of BF_3 gas at the correct intensity of 25% compared to mass 49.[26] Thus, it seems that BF_3 is the major compound which is evolved during TMB decomposition. Mechanistically, BF_3 is most likely formed by the nucleophilic attack of PF_6^- anions on the boron anion receptor of the TMB molecule, as was described for analogous boron-based anion receptors[27] and as was suggested for TMB by DFT calculations.[28] This reaction is described in scheme 1(a), namely the reaction of TMB with PF_6^- to trifluoro boroxine ($B_3F_3O_3$), CH_3^- carbanions and PF_5. In analogy to the known decomposition of boroxine ($B_3H_3O_3$) to BH_3 and B_2O_3,[29] it is reasonable to assume that trifluoroboroxine will decompose to BF_3 and B_2O_3, as is shown in scheme 1(b). As a next step in the TMB decomposition, one might consider the work by Smolanoff et al.,[30] who showed that B_2O_3 reacts with HF, evolving BF_3 gas and H_2O (scheme 1(c)). The latter is known to react readily with both PF_6^- and PF_5 to HF and POF_3 (scheme 1(d)).[24,25]

If schemes 1(a)–1(c) were correct, we would expect to see mass signals for POF_3, HF, and/or PF_5. As a matter of fact, Figure 6d shows the evolution of the 85 and 19 signals, attributed to POF_3 and HF, respectively (note that their intensity in the absence of TMB

Table II. Fitting parameters from EIS spectra shown in Figure 4 at the end of 1st and 20th discharge in electrolyte containing 0%, 0.2% and 0.5% TMB. Fit 1 and fit 2 refer to numerical fits of the equivalent circuit model shown in Figure 5, using the same data set but different initial estimates for the numerical fit.

	Fit 1				Fit 2			
Ω.cm^2	$R_{electrolyte}$	R_{SEI}	R_{CT}	($R_{SEI} + R_{CT}$)	$R_{electrolyte}$	R_{SEI}	R_{CT}	($R_{SEI} + R_{CT}$)
no TMB / 1st cycle	3.0	1.5	6.7	8.2	3	3.5	7.0	10.5
no TMB / 20th cycle	4.5	2.3	9.4	11.7	4.5	3.2	11.4	14.6
0.2% TMB / 1st cycle	0.8	1.1	7.9	9.0	0.8	8.6	7.4	16.0
0.2% TMB / 20th cycle	0.8	1.5	9.5	11.0	0.8	11.0	3.5	14.5
0.5% TMB / 1st cycle	4.5	36	93	129	4.5	109	3.1	112
0.5% TMB / 20th cycle	4.5	381	2471	2852	4.5	2247	306	2253

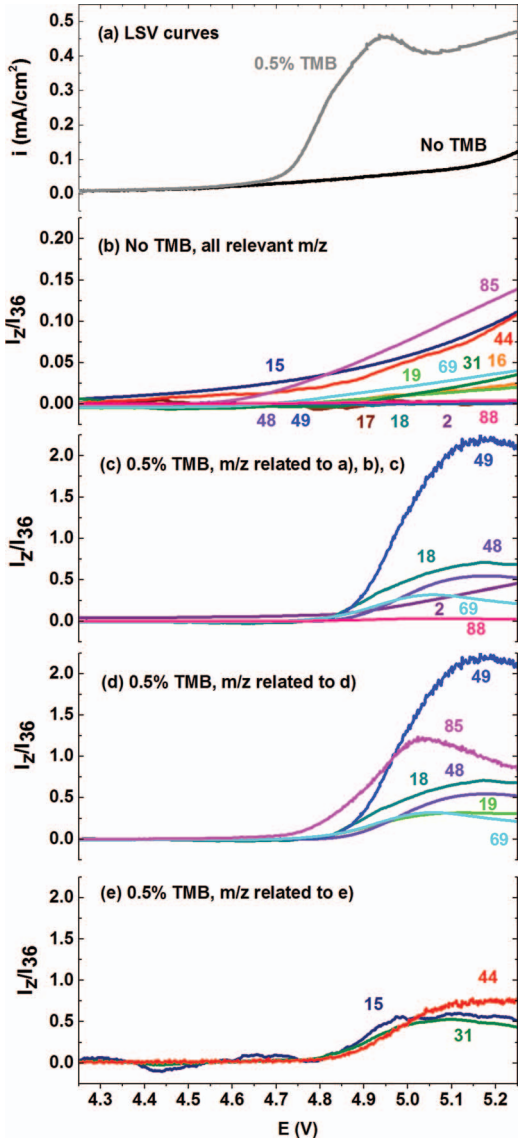

Figure 6. Current densities and OEMS signals obtained during a linear voltammetric scan (0.2 mV/s) on a carbon electrode in electrolyte electrolyte (1 M $LiPF_6$ in EC:DMC (1/1 g/g)) containing no TMB and containing 0.5% TMB: a) voltammetric current vs. potential; b) mass signals normalized to the ^{36}Ar isotope signal, I_Z/I_{36}, in electrolyte containing no TMB; c-e) mass signals in electrolyte containing 0.5% TMB. The corresponding species and the proposed reaction mechanism are shown in scheme 1(a)–1(e).

is an order of magnitude lower as shown in Figure 6b). The production of POF_3 is confirmed by the concomitant evolution of the 69 signal, which is a fragment of POF_3 with an expected intensity of ≈20% compared to mass 85.[26] In summary, the balance equation of the above proposed TMB decomposition reactions (scheme 1(a)–1(d)) is presented in scheme 1 as the "in sum" reaction, suggesting that TMB reacts with PF_6^- anions to BF_3, POF_3 and CH_3^- carbanions. This is consistent with the observation of gaseous BF_3 and POF_3 as well as with the absence of significant amounts of PF_5 (mass 88). It is noteworthy, that this balance equation would suggest that TMB can be decomposed completely into BF_3 and POF_3. Additionally, the evolution of the water signal (mass 18) follows that of POF_3 and BF_3 (Figure 6c–6d), which indicates that its formation is related to TMB oxidation. The evolution of the mass signal 2, corresponding to H_2 production, confirms the production of water since water is known to get reduced at the lithium anode to H_2 gas and OH^-.[29]

a) $B_3(CH_3)_3O_3 + 3\ PF_6^- \rightarrow 3\ PF_{5\ (g)\ [88,\ 69]} + B_3F_3O_3 + 3\ H_3C^-$

b) $B_3F_3O_3 \rightarrow BF_{3\ (g)\ [\underline{49},\ 48]} + B_2O_3$

c) $B_2O_3 + 6\ HF_{\ [19]} \rightarrow 2\ BF_{3\ (g)\ [\underline{49},\ 48]} + 3\ H_2O_{\ [\underline{18},\ 17]}$

d) $3\ H_2O_{\ [\underline{18},\ 17]} + 3\ PF_{5\ [88,\ 69,\ 50]} \rightarrow 6\ HF_{\ [19]} + 3\ POF_{3\ (g)\ [\underline{85},\ 69]}$

in sum: $B_3(CH_3)_3O_3 + 3\ PF_6^- \rightarrow 3\ BF_3 + 3\ POF_3 + 2\ H_3C^-$

e) $H_3C^- + C_3H_4O_3\ (EC) \rightarrow CO_{2\ (g)\ [\underline{44}]} + H_3C\text{-}CH_2\text{-}CH_2\text{-}O^-\ [31]$

Scheme 1. Proposed mechanism of the TMB decomposition reaction pathway. Numbers in square brackets indicate the expected main mass signals (underlined numbers represent main mass peak(s), others represent secondary peak(s)).

However, other relevant mass signals are evolved during the LSV experiment (Figure 6e), which have not been discussed yet. These are masses 44, 31, and 15, which have a very similar evolution pattern and thus seem to be related. Mass signal 44 is likely due to CO_2 and mass signal 31 is characteristic of n-alcohols;[26] while mass 15 could derive from CH_4, this does not seem possible, since it would require an equally strong signal on mass 16; so that we currently cannot identify the species detected on mass 15. CO_2 (mass 44) and alcohol (mass 31) evolution could be explained by a mechanism analogous to the nucleophilic attack of CH_3^- carbanions on the carbon atom in ethylene oxide shown in scheme 1(e), analogous to the nucleophilic attack of OH^- anion on the carbon atom in EC described by Aurbach.[31] Thus, we hypothesize that the carbanion produced by the TMB oxidation (scheme 1(a)) decomposes the carbonate solvents of the electrolyte through a similar mechanism, resulting in the formation of CO_2 and propanol (scheme 1(e)).

Discussion

The presented study suggests that TMB decomposes at ≥4.5 V by producing large amounts of BF_3, POF_3, and CO_2 as well as H_2O and H_2. These results would be in accordance with the study by Sharabi et al.,[15] in which it was shown by XPS that TMB additive leads to higher amounts of fluorophosphates ($P_xO_yF_z$ or $Li_wP_xO_yF_z$) on the LCP surface while no boron surface species could be detected. The former would likely be created through the reaction of POF_3 with the LCP surface while the absence of boron surface species can be explained by the preferential formation of BF_3. Again, for the completion of the sequence of schemes 1(a)–1(d), only trace amounts of HF or water would be required.

The increased mass signal for water (mass 18) with increasing potential suggests that another factor, caused by the decomposition products of TMB, is responsible for water and/or HF production. In the Figure 6c, the signals corresponding to BF_3 (49 and 48) seem to decrease at the end of the LSV and the trend is confirmed since the experiment was made until 5.5 V (not shown). A significant decrease of the intensity I_Z/I_{36} is correlated with a consumption of the produced gases. Gasselin[32] demonstrated that boron trifluoride, which can be considered as a Lewis acid, is a highly reactive compound. Many reactions are described but, however, no clear conclusion can be made about the origin of water and/or HF during the TMB oxidation. The analysis of ICL and CV are suggested that an optimum amount of TMB is needed to passivate the electrode. An excess of TMB shows higher degradation currents and bigger ICL values. Probably, the high amount of the side reaction products from TMB decomposition (H_2O, HF and BF_3) could be responsible of the fading mechanism of LCP half-cell. Also, the interaction with the counter electrode cannot be neglected since H_2 coming from the reactivity of lithium metal with water is evolved.

The electrochemical and chemical decomposition of TMB was described. However, the improved electrochemical performance showed by Sharabi[15] on LCP is still an open question. It was mentioned in the work by Reddy et al.[27] that the first step of TMB decomposition allows the polymerization of carbonates in the electrolyte due to the catalytic effect of PF_5. Moreover, Rokicki et al.[33] showed that the reaction between oxiranes and carbonates, which leads to poly(ether-carbonate)s, is enhanced by the presence of the complexe BF_3-Et_2O. The catalytic activity of BF_3 and/or PF_5 on the carbonates could coat faster the surface of LCP particles and avoid the degradation of the material that is responsible for the poor electrochemical performance.[13] Also, it is not excluded that the formation of the propanol, found in the OEMS experiment, plays a role in the polymerization of carbonates.[34] Interestingly, the EIS study shows a huge resistance in presence of 0.5% TMB. Considering the high amount of TMB oxidation products, it could be correlated to a thick layer of carbonate polymers. Since the electrolyte containing 0.2% TMB shows a similar resistance compared to the electrolyte without TMB, the earlier decomposition of TMB, before the electrochemical oxidation of LCP, could be a key factor in the SEI formation. However, a careful XPS study is needed to understand if the TMB decomposition leading to an earlier passivation on the cathode is a reasonable hypothesis for explaining the good capacity retention of LCP.

Conclusions

The combination of CV, EIS and OEMS techniques allows the understanding of the additive decomposition at high voltage. It is shown that TMB decomposes at $\geq$4.5 V essentially to BF_3, POF_3 and carbanion. A complete mechanism is proposed. However, two questions cannot be answered and further investigations are needed. On the one hand, the origin of water and/or HF production during the decomposition of TMB cannot be explained. On the other hand, the reason for a better cycling stability of LCP in presence of TMB is not clear. It is suspected that TMB decomposition products (BF_3 and/or PF_5) can catalyze the polymerization of carbonates and subsequently, the formation of a protective layer which happens earlier in the LCP charge. Impedance results seem to correlate this assumption but a careful XPS study should bring more information.

Acknowledgments

We thank BMW AG for its financial support, Dr. Himendra Jha for his helpful discussion and Katia S. Rodewald for the SEM picture.

References

1. H. Ikeda, S. Uena, T. Saito, S. Nakaido, and H. Tamaru, *Denki Kagaku*, **45**, 391 (1977).
2. M. S. Whittingham, *J. Electrochem. Soc.*, **123**, 315 (1976).
3. K. Ozawa, *Solid State Ionics*, **69**, 212 (1994).
4. M. S. Whittingham, *Chem. Rev.*, **104**, 4271 (2004).
5. A. K. Padhi, K. S. Nanjundaswamy, and J. B. Goodenough, *J. Electrochem. Soc.*, **144**, 1188 (1997).
6. K. Zaghib, A. Guerfi, P. Hovington, A. Vijh, M. Trudeau, A. Mauger, J. B. Goodenough, and C. M. Julien, *J. Power Sources*, **232**, 357 (2013).
7. N. Bramnik, K. Bramnik, T. Buhrmester, C. Baehtz, H. Ehrenberg, and H. Fuess, *J. Solid State Electrochem.*, **8**, 558 (2004).
8. S. Brutti and S. Panero, *Nanotechnology for Sustainable Energy* (ACS Symposium Series), Chap4, 68 (2013).
9. J. Ni, H. Wang, L. Gao, and L. Lu, *Electrochimica Acta*, **70**, 349 (2012).
10. S. M. Oh, S. T. Myung, and Y. K. Sun, *J. Mater. Chem.*, **22**, 14932 (2012).
11. R. E. Rogers, G. M. Clarke, O. N. Matthew, M. J. Ganter, R. A. Dileo, J. W. Staub, M. W. Forney, and B. J. Landi, *J. Appl. Electrochem.*, **43**, 271 (2013).
12. Y. M. Kang, Y. I. Kim, M. W. Oh, R. Z. Yin, Y. Lee, D. W. Han, H. S. Kwon, J. H. Kim, and G. Ramanath , *Energy Environ. Sci.*, **4**, 4978 (2011).
13. E. Markevich, R. Sharabi, H. Gottlieb, V. Borgel, K. Fridman, G. Salitra, D. Aurbach, G. Semrau, M. A. Schmidt, N. Shall, and C. Bruenig, *Electrochem. Comm.*, **15**, 22 (2012).
14. R. Sharabi, E. Markevich, V. Borgel, G. Gershinsky, G. Salitra, D. Aurbach, G. Semrau, M. A. Schmidt, N. Schall, and C. Stinner, *J. Power Sources*, **203**, 109 (2012).
15. R. Sharabi, E. Markevich, K. Fridman, G. Gershinsky, G. Salitra, D. Aurbach, G. Semrau, M. A. Schmidt, N. Schall, and C. Bruenig, *Electrochem. Comm.* **28**, 20 (2013).
16. N. Tsiouvaras, S. Meini, I. Buchberger, and H. A. Gasteiger, *J. Electrochem. Soc.*,**160**, A471 (2013).
17. I. C. Jang, H. H. Lim, S. B. Lee, K. Karthikeyan, V. Aravindan, K. S. Kang, W. S. Yoon, W. I. Cho, and Y. S. Lee, *Journal of Alloys and Compounds*, **497**, 321 (2010).
18. V. Petricek, M. Dusek, and L. Palatinus, JANA 2006, *Z. Kristallogr.* **229**(5), 345 (2014).
19. N. Bramnik, K. Nikolowski, C. Baehtz, K. G. Bramnik, and H. Ehrenberg, *Chem. Mater.*, **19**, 908 (2007). S. S. Zhang and T. R. Jow, *J. Power Sources*, **109**, 458 (2002).
20. A. Rajalakshmi, V. D. Nithya, V. D. Karthikeyan, C. Sanjeeviraja, Y. S. Lee, and R. K. Selvan, *J. Sol-Gel Sci. Technol*, **65**, 399 (2013).
21. R. Imhof and P. Novak, *J. Electrochem. Soc.*, **146**, 1702 (1999).
22. F. Joho and P. Novak, *Electrochimica Acta*, **45**, 3589 (2000).
23. C. L. Campion, W. Li, and B. L. Lucht, *J. Electrochem. Soc.*, **152**, A2327 (2005).
24. K. Xu, *Chem. Rev.*, **104**, 4303 (2004).
25. M. S. Lee, *Mass Spectrometry Handbook*, (2012).
26. V. P. Reddy, M. Blanco, and R. Bugga, *J. Power Sources*, **247**, 813 (2014).
27. O. Borodin and T. R. Jow, *224th ECS Meeting*, Abstract#1181 (2013).
28. L. Barton, *J. Inorg. Nucl. Chem.*, **30**, 1683 (1968).
29. J. Smolanoff, A. Lapicki, N. Kline, and S-L. Anderson, *J. Phys. Chem.*, **99**, 16276 (1995).
30. D. Aurbach, *Nonaqueous Electrochemistry*, p. 145, 146, 205, Marcel Dekker Inc., New York/Basel (1999).
31. J. Gasselin, *Annal. Chim. Phys.*, **7**, 5 (1894).
32. G. Rokicki and T. X. Nguyen, *J. Macromol. Sci. part A: Pure Appl.Chem.*, **32**(3), 265 (1995).
33. A.G. Shaikh and S. Sivaram, *Chem. Rev.*, **96**, 951 (1996).